ELSEVIER

J. Non-Newtonian Fluid Mech. 102 (2002) 135–148

Journal of Non-Newtonian Fluid Mechanics

www.elsevier.com/locate/jnnfm

Rotational dynamics in dipolar colloidal suspensions: video microscopy experiments and simulations results

Sonia Melle [a,b,c,*], Oscar G. Calderón [b], Miguel A. Rubio [b], Gerald G. Fuller [a]

[a] *Department of Chemical Engineering, Stanford University, Stanford, CA 94305-5025, USA*
[b] *Dpto. Física Fundamental, UNED, Senda del Rey 9, Madrid 28040, Spain*
[c] *Dpto. Optica, UCM, Ciudad Universitaria s/n, Madrid 28040, Spain*

Abstract

The dynamics of field-induced structures in very dilute dipolar colloidal suspensions subject to rotating magnetic fields have been experimentally studied using video microscopy. When a rotating field is imposed the chain-like aggregates rotate with the magnetic field frequency. We found that the size of the induced structures at small rotational frequencies is larger than at zero rotating frequency, i.e. when an uniaxial magnetic field is applied. At higher frequencies, the average size of the aggregates decreases with frequency following a power law with exponent −0.5 as the hydrodynamic friction forces overcome the dipolar magnetic forces, causing the chains break up. A non-thermal molecular dynamics simulations are also reported, showing good agreement with the experiments.

Keywords: Magnetorheological fluids; Rotating magnetic fields; Aggregation processes

1. Introduction

Magnetic fluids exhibit interesting dynamical behavior when subjected to rotating magnetic fields as has been reported in previous experimental studies on magnetic holes [1,2], magnetic droplets [3,4] and magnetorheological (MR) suspensions [5,6]. Similar to the behavior of liquid crystals [7,8], these systems show synchronous and non-synchronous regimes depending on the value of the driving frequency. Helgesen et al. [1,2] studied the response of a pair of magnetic holes subjected to rotating fields. They found a transition between a uniform rotation of the pair phase-locked to the field at low rotational frequencies, to a forward–backward rotation with additional radial oscillations each time the axis between the holes rotates opposite to the field. For a pair of magnetic particles immersed within a fluid,

* Corresponding author.
E-mail address: smelle@fisfun.vned.es (S. Melle).
Dedicated to Professor Acrivos on the occasion of his retirement from the Levich Institute and the CCNY.

0377-0257/02/$ – see front matter
PII: S0377-0257(01)00174-4

Kashevsky and Novokova [5] found that the plane of the magnetic field rotation is the attractive one for the pair motion. Bacri et al. [3] found unexpected spiny, starfish shaped magnetic micro-droplets co-rotating with the field for high rotational frequencies. At lower frequencies, Sandre et al. [4] found that the magnetic micro-droplets break up to decrease their viscous drag and facilitate tracking the field rotation.

In our previous work [6], we studied the orientation dynamics of dilute MR suspensions ($\phi \simeq 0.016$) using scattering dichroism. In these suspensions, dichroism is caused by the polarization dependent scattering from oriented aggregates [9]. The time evolution of the dichroism and the orientation angle of the structures were measured simultaneously and it was observed that the structures followed the rotating magnetic field with a phase lag that was independent of time for all frequencies measured. This phase difference increased with frequency over the whole range of frequencies.

In order to simulate MR suspensions, algorithms have been developed incorporating Stokes friction, magnetic interaction, excluded-volume force, and Brownian motion [10–13]. In some cases, the magnetic interaction of the particles dominates their random thermal motion [14,15]. To quantify the relative importance of these two effects, the dimensionless ratio of the magnetic inter-particle interaction energy and the thermal energy is considered. This ratio is $\lambda \equiv W_{\mathrm{m}}/k_{\mathrm{B}}T = \mu_0 m^2/16\pi a^3 k_{\mathrm{B}}T$, where μ_0 is the vacuum magnetic permeability, m the magnetic moment of the particle, a the radius of the particle, k_{B} the Boltzman constant, and T the temperature. In our experiments, this ratio is on the order of $\lambda \simeq 700$. In this regime, Martin et al. [15] developed 3D molecular dynamics simulations of colloidal suspensions subjected to high frequency biaxial fields. They predicted the formation of particles into 2D, sheet-like structures aligned in the field plane when the frequency of the field is sufficiently high so that particles migrate less than their own diameter during a field cycle.

For concentrated suspensions of spherical particles under simple shear flow, an specially accurate method called Stokesian dynamics (SD) has been developed by Bossis and Brady [16]. They replaced the simple Stokes law for the drag force on a sphere by a more accurate tensor expression that accounts for the hydrodynamic interactions, i.e. the disturbances to the solvent velocity field produced by the relative motions of the other spheres. Bonnecaze and Brady [17] modified the SD method to include multipole and multibody effects in order to simulate electrorheological fluids under simple shear. Latter on, thermal fluctuations were added [18]. SD simulations of ferromagnetic colloidal dispersions in simple shear have been also conducted by Satoh et al. [19].

In this work, we report on an experimental video microscopy study of the aggregation and orientation dynamics in very dilute suspensions ($\phi \simeq 5 \times 10^{-4}$) of magnetic dipolar particles under rotating magnetic fields. We analyze the behavior of the average length of the chain-like structures induced by the rotating magnetic field. We found that the sizes of the structures induced at small frequencies are larger than at zero rotating frequency, i.e. when a uniaxial magnetic field is applied. However, at higher frequencies, the average size of the aggregates decreases with frequency following a power law behavior with an exponent close to -0.5.

In order to understand the dynamics governing structure formation in MR suspensions under rotating magnetic fields a first-order approach has been used [14,15,20]. Therefore, we considered in our simulations only those effects that we believe are essential to capture the main features found in our experiments. Since $\lambda \gg 1$, we developed a thermal molecular dynamics simulations of "hard" spheres with induced dipolar interactions and Stokes friction against the solvent. Comparison of the experimental results with the simulations results shows good agreement indicating that our simple model accounts for the essential physics involved in the dynamics.

2. Experimental materials and procedure

To study the dynamics governing low volume fraction dipolar suspensions under the application of rotating magnetic fields we performed video microscopy experiments for an aqueous suspension of super-paramagnetic latex micro-spheres loaded with iron oxide grains.

2.1. Magnetic suspension

In the experiments reported here, we used an aqueous magnetic suspension (d-M1-180/20) obtained diluting a 10% in weight suspension supplied by *Estapor* (M1-180/20) to achieve a volume fraction $\phi = 5 \times 10^{-4}$. The properties of the magnetizable particles making up this suspension are detailed in Table 1. These particles content magnetite crystals (Fe_3O_4) of small diameter (1–20 nm) dispersed in a monomer—divinylbenzene (DVB)—and polymerized using a emulsion process. The surface of the latex micro-spheres is composed of carboxylic acid (–COOH) groups with an added surfactant coating layer of sodium dodecyl sulfate (SDS) to stabilize the dispersions. In order to avoid particle aggregation in the dilution process additional SDS was applied. Since these iron oxide grains are randomly oriented inside the micro-particles, the resulting magnetic moment is zero in the absence of an external magnetic field. When a magnetic field is applied, a net magnetic dipolar moment aligned in the field direction is induced in the particles as a result of the orientation of the grains dispersed in the polymer matrix. This magnetic moment is $\vec{m} = (4\pi/3)a^3\vec{M}$, with $\vec{M}$ the magnetization of the particle. We have characterized the average magnetic properties of the particles by measuring their magnetization curve using a vibrating sample magnetometer (VMS-*Lakeshore* 7300). We observed that under sufficiently low magnetic fields these particles exhibit superparamagnetic behavior with virtually no hysteresis or magnetic remanence. Due to their small average diameter and density ($\rho_p \approx 1.3$ g/ml) the sedimentation time is long enough to neglect gravitational effects. The sedimentation velocity was estimated according to Stokes' law to be $v_s = 0.02\,\mu$m/s.

2.2. Sample cell

Because the technique used here requires optical transparency, the fluid sample was sandwiched between two circular quartz windows with i.d. 6.5 mm. These windows were held in place by a delrin attachment designed to prevent evaporation of the solvent and separated by an annular delrin spacer $e = 100\,\mu$m thick along the light path axis, Z (see Fig. 1). The video microscopy images were taken at an area in the cell <0.1 mm in the vicinity of the center. The sample is surrounded by two orthogonal pairs of coils

Table 1
Properties of the magnetic latex micro-spheres used

Original suspension	M1-180/20
Mean diameter (μm)	0.87
Magnetic content (%)	24.8
Saturation magnetization (emu/g)	21
Polymer nature	DVB
Surface groups –COOH content (μeq./g)	53

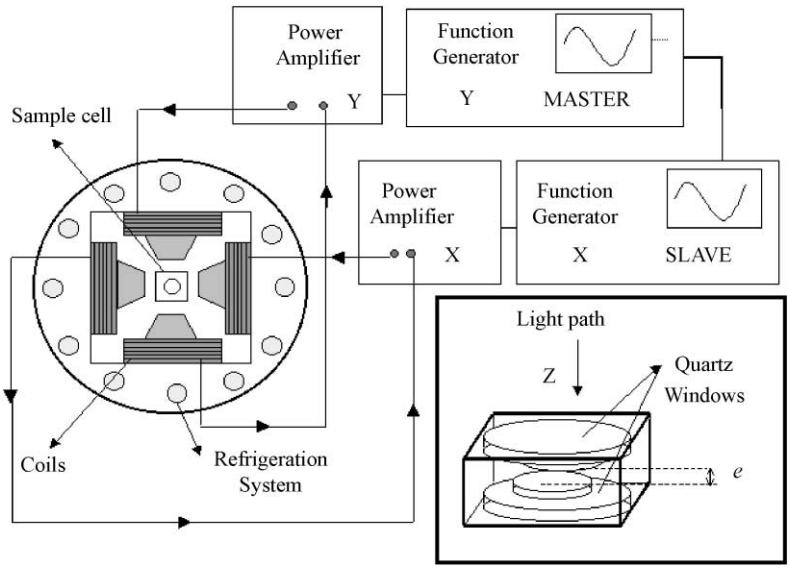

Fig. 1. Sketch of the coils system (from the direction of the light path) to produce a rotating magnetic field in the sample. On the right down corner, the quartz magnetic suspension cell is shown.

that generate a rotating magnetic field in the plane of the images (*XY*). The rotating magnetic field was achieved by applying sinusoidal electric signals to the two orthogonal pairs of coils by means of two Kepco BOP20-10M power amplifiers, driven by two HP-FG3325A function generators referenced to one another at a phase difference of 90° (see Fig. 1). The function generators allowed for control of both the amplitude and the frequency of the rotating magnetic field. These coils are housed in a temperature controlled aluminum cylinder to prevent heating effects. All experiments were performed at a temperature of $T = (282 \pm 1)$ K on the sample. The coils relative positions and their dimensions were optimized to obtain the smallest spatial variation of the field over the sample (<3%). This minimized local changes of concentration due to the transport of the magnetic latex particles under the effect of field gradients. In Table 2 are summarized the experimental conditions.

2.3. Video microscopy set-up

The video microscopy set-up is shown in Fig. 2. The sample cell surrounded by the four coils is situated in the horizontal plane (*XY*), and the optical train (in the direction of the *Z*-axis) consists of a light source

Table 2
Summary of the experimental conditions

Diluted suspension	d-M1-180/20
Final volume fraction, ϕ	5×10^{-4}
Magnetic field strength, H_0	12.4 kA/m
Rotational frequencies range, f_0	0.001–2 Hz

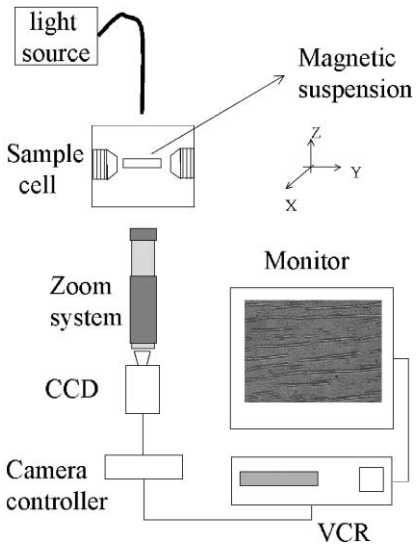

Fig. 2. Depiction of the video microscopy set-up showing the sample cell with the coils situated in the horizontal plane, and the vertical optical train consisting of a light source, a zoom system and a CCD video camera connected to the VCR.

with flexible bundle (*American Optical* II-80), a zoom system (*Navitar* 12×) and a CCD video camera (*Sanyo* VDC-3825) connected to a S-VHS VCR (*Panasonic* AG 1975). The *Navitar* 12× Zoom System is compose of a 2× adapter that attaches the CCD camera to the zoom, a 12× zoom, and a 2× attachment that joins the zoom to a 10× microscope objective. This group of lens' provides a combination of a large zoom range with high resolution. This zoom system has the capability of allowing the field of view to be altered by changing the image resolution. A resolution of 0.34–4.2 μm for field of view around 170–2100 μm was possible with this system.

2.4. Experimental procedure and image processing

A typical experimental protocol would begin with a homogeneous sample and then apply the rotating magnetic field for 365 s. Although the zoom magnification was varied for each experiment to adapt the field of view, a resolution that allow us to see individual particles was always used. As a result, at small frequencies, the field of view was not of sufficient magnitude to visualize the number of structures necessary to obtain a good statistics for the average magnitudes of aggregate length and orientation.

During the time the field was applied images were recorded using a VCR at 30 frames per second. We subsequently digitalized single frames of 640 pixels × 480 pixels with 256 grey levels on a computer (DT-2862) at fixed time intervals depending on the field rotational frequency. To analyze the digitalized images we used *Igor Pro* image-processing software. The images had a dark background over which the particles appear as clear areas. To calculate the length of the chains the pixel area for each aggregate was calculated by applying a grey level threshold that was kept constant for a given experiment. Then, the temporal evolution of the average length was determined. The average rotation angle of the chains was also computed by analyzing the Hough Transform of the images [21,22].

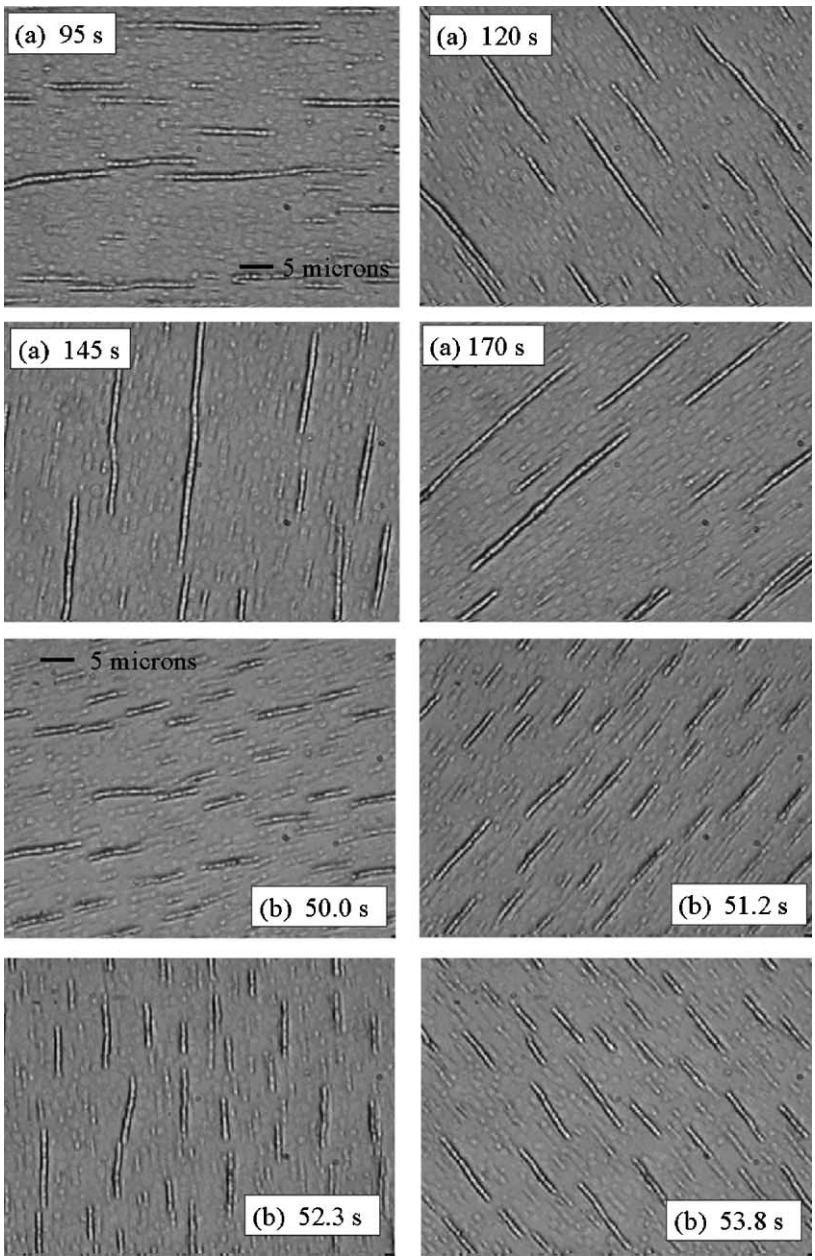

Fig. 3. Quarter cycle of the time evolution of the fibrillated structures for different rotational frequencies: (a) $f_0 = 0.005\,\mathrm{Hz}$ clockwise rotation; (b) $f_0 = 0.1\,\mathrm{Hz}$ counter clockwise rotation. Field of view: $62\,\mu\mathrm{m} \times 46\,\mu\mathrm{m}$.

3. Experimental results

In Fig. 3, video microscopy images show the temporal evolution of the structures that appear when a rotating magnetic field with amplitude $H_0 = 12.4\,\text{kA/m}$ was applied for two different rotational frequencies. When the magnetic field is first applied, a magnetic dipole is induced in each particle in the direction of the field. At this low volume fraction ($\phi = 0.0005$) the dipolar interaction induces particle aggregation into linear chains that follow the magnetic field direction. Under these conditions, two torques act on the aggregates: a magnetic torque that rotates the chain-like structures due to dipolar interaction among the particles oriented in the direction of the magnetic field, and a hydrodynamic torque caused by the rotational friction of the structures in the suspending fluid. We can see in Fig. 3 how the length of the structures is larger for slower rotational frequencies. In the rotation process, we observed continuous fragmentation and aggregation of chains for all the frequencies.

The chains rotate synchronously with the applied field for the range of frequencies measured (between $f_0 = 0.001$ and 2 Hz), but break up to decrease their viscous drag. As an example of this synchronous rotation, in Fig. 4, we plot the time evolution of the average angle for a rotating field frequency of $f_0 = 0.005\,\text{Hz}$. The average rotational frequency measured for the aggregates was $f_{\text{chains}} = 0.0052\,\text{Hz}$. This synchronous regime was also observed for more concentrated suspensions [6]. In that work, we also measured the phase lag between the aggregates and the field using scattering dichroism. As expected, the longer the aggregates, the higher is their phase lag.

The time evolution of the average length of the chains for different rotational frequencies was also studied. As an example, the temporal evolution of the average length of the chains at the smaller rotating frequency of $f_0 = 0.001\,\text{Hz}$ is plotted in Fig. 5. One can see that after a time of approximately 150 s the average chain length reaches a steady value (around 25 particles). The time necessary to reach the steady state decreases when the rotational frequency increases.

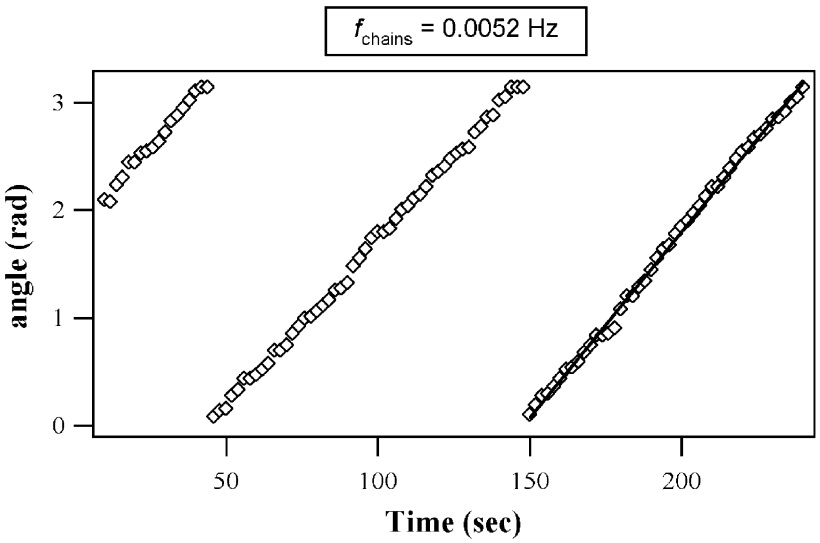

Fig. 4. Time evolution of the average orientation angle for the fibrillated structures induced when a rotating magnetic field of frequency $f_0 = 0.005\,\text{Hz}$ is applied. The structures synchronously rotate with the field.

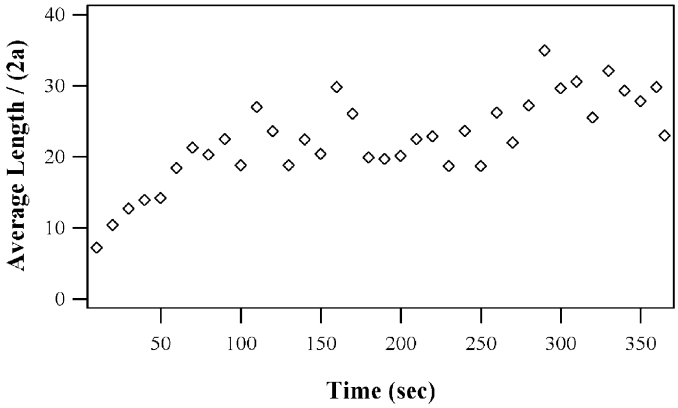

Fig. 5. Temporal evolution of the chains average length for a magnetic field with amplitude $H_0 = 12.4\,\text{kA/m}$ and frequency $f_0 = 0.001\,\text{Hz}$.

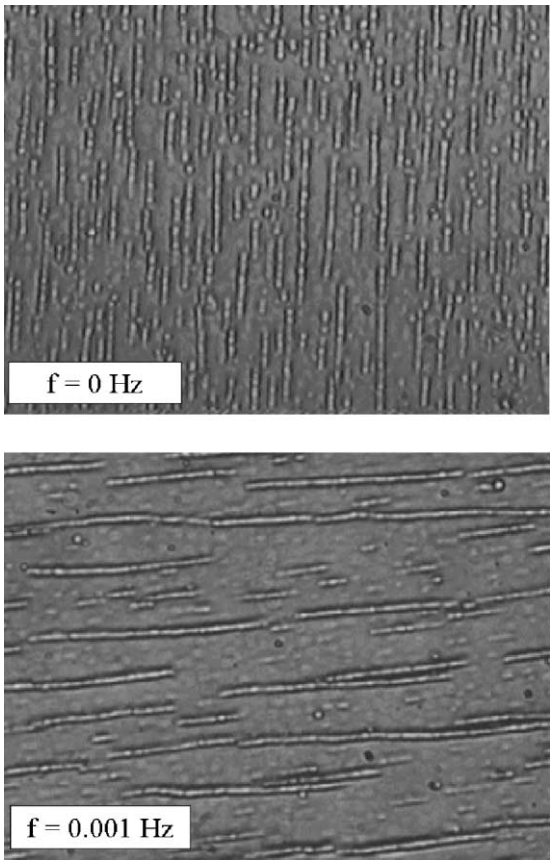

Fig. 6. Video microscopy images recorded at time $= 180\,\text{s}$ after applying a magnetic field with amplitude $H_0 = 12.4\,\text{kA/m}$. Chain-like structures induced at zero frequency, $f_0 = 0.0\,\text{Hz}$, (upper image); and at rotational frequency $f_0 = 0.001\,\text{Hz}$ (lower image). Field of view: $76\,\mu\text{m} \times 57\,\mu\text{m}$.

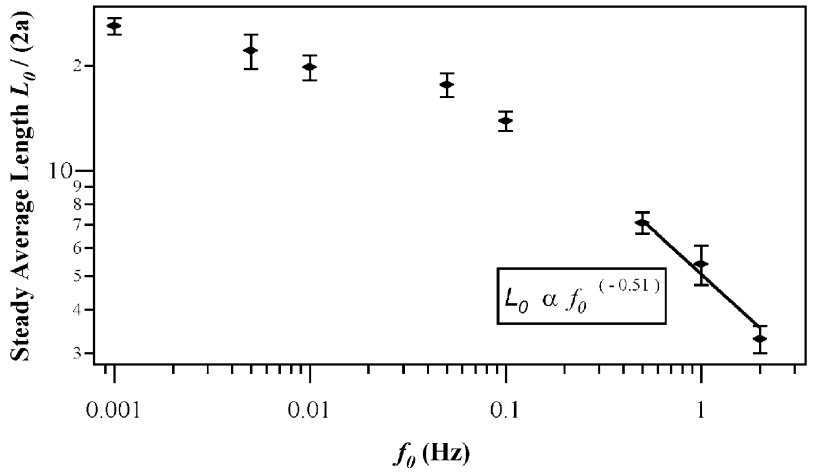

Fig. 7. Variation of the steady average length of the aggregates with the rotational frequency. At higher frequencies the average length follows a power law with exponent −0.51.

Studying the temporal evolution of the chains average length we found that for a given time, this average length is enlarged for low rotational frequencies ($f_0 = 0.001$ Hz) compares to the case of unidirectional constant magnetic fields $f_0 = 0.0$ Hz. This fact can be seen in Fig. 6 where video microscopy images taken at the same time shown larger length for low frequencies than for zero frequency. So the fact that the chains are rotating is helping to the aggregation process. However, when we increase more the frequency, the average length of the structures starts decreasing indicating that viscous drag becomes more important.

In Fig. 7, we plotted the variation of the stationary average length with the rotational frequency. We see how the steady average length of the structures decreases with the rotational frequency for all the frequencies measured. Furthermore, at higher frequencies, the average size strongly decreases with frequency following a power law with exponent −0.51 due to the hydrodynamic friction forces overcome the dipolar magnetic forces and, therefore, the chains break up to decrease their viscous drag. For these high frequencies the viscous drag is restricting the size of the structures.

4. Theory

4.1. Theoretical model

In order to interpret the experimental results, we developed a non-thermal 2D molecular dynamics simulations of "hard" spheres with induced dipolar interactions and Stokes friction against the solvent. We consider a monodisperse suspension of N spherical particles with radius a in water subjected to a rotating magnetic field in the XY plane with rotational frequency f_0

$$\vec{H} = H_0(\cos(2\pi f_0 t)\hat{x} + \sin(2\pi f_0 t)\hat{y}). \tag{1}$$

A complete algorithm to simulate such a system would include Brownian motion, multipolar magnetic interaction forces between the particles, local field corrections to the applied field, hydrodynamic friction

forces (lubrication and long range), excluded-volume repulsive forces, and so on. However, as we have already pointed out, our approach has been to consider only those contributions we believe are essential to capture the physics of the problem. Similar approaches have been previously used to simulate MR fluids [14,15], as well as electrorheological fluids [20].

Taking into account that the aggregation takes place in the plane of the magnetic field rotation [5], we simplified our calculations by developing 2D simulations in this plane. For the magnetic field used in the experiments ($H_0 = 12.4\,\mathrm{kA/m}$) the magnetization of the particle was measured to be $M = 8.6\,\mathrm{kA/m}$ being its dipolar moment $m \simeq 3 \times 10^{-15}\,\mathrm{A\,m^2}$. Furthermore, one can estimate the magnetic interaction energy between dipoles as the energy required to separate two magnetized particles in contact along the field direction. Using a point-dipole approximation, this energy will be $\mu_0 m^2/16\pi a^3 \simeq 3 \times 10^{-18}\,\mathrm{J}$. On the other hand, the thermal energy at the temperature of the experiments ($T = 282\,\mathrm{K}$) $k_\mathrm{B}T = 4 \times 10^{-21}\,\mathrm{J}$, is much smaller than the magnetic energy so that Brownian motion should have a negligible effect on the evolution of the structures [23]. In other words, the key dimensionless parameter mentioned in the introduction that measures the ratio between the magnetic and thermal energies will be much larger than one, $\lambda \equiv W_\mathrm{m}/k_\mathrm{B}T \simeq 700$.

Under these assumptions, the equation of motion for the ith particle is

$$m\frac{\mathrm{d}^2\vec{r}_i}{\mathrm{d}t^2} = \vec{F}_i^{\,\mathrm{v}} + \vec{F}_i^{\,\mathrm{m}} + \vec{F}_i^{\,\mathrm{ev}}, \tag{2}$$

where m is the particle mass, $\vec{r}_i$ the position of the ith particle, $\vec{F}_i^{\,\mathrm{v}}$ the viscous force, $\vec{F}_i^{\,\mathrm{m}}$ the magnetic force, and $\vec{F}_i^{\,\mathrm{ev}}$ the excluded-volume force. The simulations can be greatly simplified by making two approximations on the viscous and the magnetic force. First, we are using Stokes' drag approximation $\vec{F}_i^{\,\mathrm{v}} = -\gamma\vec{v}_i$, where $\gamma = 6\pi\eta a$ is the Stokes drag coefficient for a solid sphere of radius a moving in a liquid with viscosity η and $\vec{v}_i$ is the particle velocity. Second, we use point-dipole approximation to compute the magnetic force acting on the ith particle. This force will be the result of the sum of the dipolar forces exerted by all the other particles, i.e.

$$\vec{F}_i^{\,\mathrm{m}} = \frac{3\mu_0 m^2}{4\pi}\sum_{j\neq i}\frac{1}{R_{ij}^4}\{[1-5(\hat{m}\,\hat{R}_{ij})^2]\hat{R}_{ij} + 2(\hat{m}\,\hat{R}_{ij})\hat{m}\}, \tag{3}$$

where $\hat{R}_{ij} \equiv \vec{R}_{ij}/R_{ij}$ with $\vec{R}_{ij} \equiv \vec{r}_i - \vec{r}_j$, and $\hat{m} = (\cos(2\pi f_0 t)\hat{x} + \sin(2\pi f_0 t)\hat{y})$. Note that linear chains aligned in the direction of the magnetic field, cannot support a shear force as both the $\hat{R}_{ij}$ and $\hat{m}$ component are working in the same axial direction. Note that as we are using one-particle Stokes' hydrodynamics, an excluded-volume force $\vec{F}_i^{\,\mathrm{ev}}$ must be included to keep particles from overlapping. This force is calculated from [14]

$$\vec{F}_i^{\,\mathrm{ev}} = A\frac{3\mu_0 m^2}{4\pi(2a)^4}\sum_{j\neq i}\hat{R}_{ij}\exp[-\xi(R_{ij}/2a - 1)], \tag{4}$$

where we assumed $A = 2$ and $\xi = 10$. Similar repulsive forces have been used in previous work [14,20]. The parameter A is chosen in order to give zero interaction force when two particles aligned along the field direction and interacting with dipolar force (see Eq. (3)), are in contact (i.e. $R_{ij}/2a = 1$). The same condition was followed in [24]. With $\xi = 10$ the ratio between dipolar and excluded-volume forces of two particles aligned with the field reaches the value 10 (0.1) when the distance between particles increases to $R_{ij}/2a = 1.1$ (decreases to $R_{ij}/2a = 0.9$).

Neglecting the inertial term and making the particle evolution Eq. (2) dimensionless we obtain:

$$\frac{\mathrm{d}\vec{\rho}_i}{\mathrm{d}\tau} = \frac{t_\mathrm{s}}{2a\gamma}[\vec{F}_i^{\mathrm{m}} + \vec{F}_i^{\mathrm{ev}}], \tag{5}$$

where a couple of scaling parameters immediately drop out, a length scale equal to $2a$ which leads to a dimensionless spatial variable equal to $\vec{\rho}_i = \vec{r}_i/2a$, and a time scale $t_\mathrm{s} \equiv 12^2\eta/\mu_0 M^2$ which leads to a dimensionless time equal to $\tau = t/t_\mathrm{s}$. This procedure has been followed in several works [15,20,25]. Using the viscosity of the sample $\eta = 1.3\,\mathrm{mPa\,s}$ we obtain a characteristic time scale equal to $t_\mathrm{s} = 2 \times 10^{-3}\,\mathrm{s}$, so one dimensionless time unit is about a millisecond. This simulation method has been developed to predict the evolution of small systems over large times.

4.2. Simulation results

We numerically solved Eq. (2) for a system with $N = 400$ particles with an initial average separation equal to $R_{ij}(t = 0)/2a \simeq 5$.

The simulations reveal that the magnetic dipolar interaction between particles induces the formation of chain-like structures that follow the magnetic field rotating with the same frequency in agreement with the experimental findings. In Fig. 8, we plot the particles position in the *XY* plane for different frequencies at an arbitrary time. As demonstrated in this figure, the size of the structures at a slow rotating field frequency (see Fig. 8b) is larger than at zero frequency, i.e. when an uniaxial magnetic field is applied (see Fig. 8a). This result is in agreement with the experimental results and indicates that the aggregation of magnetic particles is favored when a slowly rotating magnetic field is applied. Therefore, this could

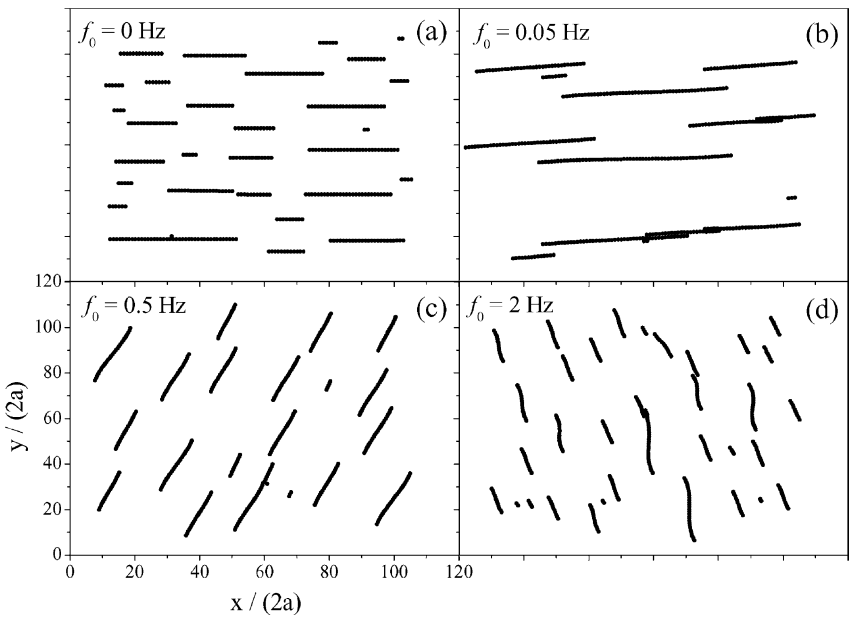

Fig. 8. Particles position in the *XY* plane at an arbitrary time, $\tau = 10{,}000$, at rotating frequency (a) $f_0 = 0\,\mathrm{Hz}$; (b) $f_0 = 0.05\,\mathrm{Hz}$; (c) $f_0 = 0.5\,\mathrm{Hz}$ and (d) $f_0 = 2\,\mathrm{Hz}$.

be a mechanism to increase the average size of the cluster in a magnetic suspension. On the other hand, at higher frequencies (see Fig. 8b–d) the size of the structures becomes smaller as the rotating frequency increases. This indicates that hydrodynamic friction forces overcome the dipolar magnetic forces and, therefore, the chains break up to decrease their viscous drag.

In order to analyze the behavior of the size of the structures we calculated the time evolution of the average length, L. This average length L was calculated considering straight chains without taking into account the shape of the clusters

$$L = \frac{\sum_j N_j}{\sum_j 1}, \tag{6}$$

where N_j is the number of particles in the jth cluster. However, it can be seen in both experimental and simulations results that chains develop an S-shape. To check its effect in our simulations results, we calculated the average length, but using a weight function $W_j = N_j s_j$, where s_j is a shape factor with value 1 for the case of a straight chain, and 0 for a symmetric cluster

$$s_j = \frac{(I_j^{\max})^{1/2} - (I_j^{\min})^{1/2}}{(I_j^{\max})^{1/2} + (I_j^{\min})^{1/2}}, \tag{7}$$

where $I_j^{\max}$ and $I_j^{\min}$ are the principal moments of inertia of jth cluster. Then, the direction of $I_j^{\min}$ gives the orientation of the long axis of the cluster. We did not observe appreciable changes in the simulations results using this shape correction. Therefore, we have presented here the results corresponding to the case without the shape factor.

In Fig. 9, the average length versus time at different rotating frequencies is plotted. After an initial transient, the average length reaches an oscillatory regime in the manner shown below.

$$L(t) \simeq L_0 + \Delta L \sin(2\pi f_L t), \tag{8}$$

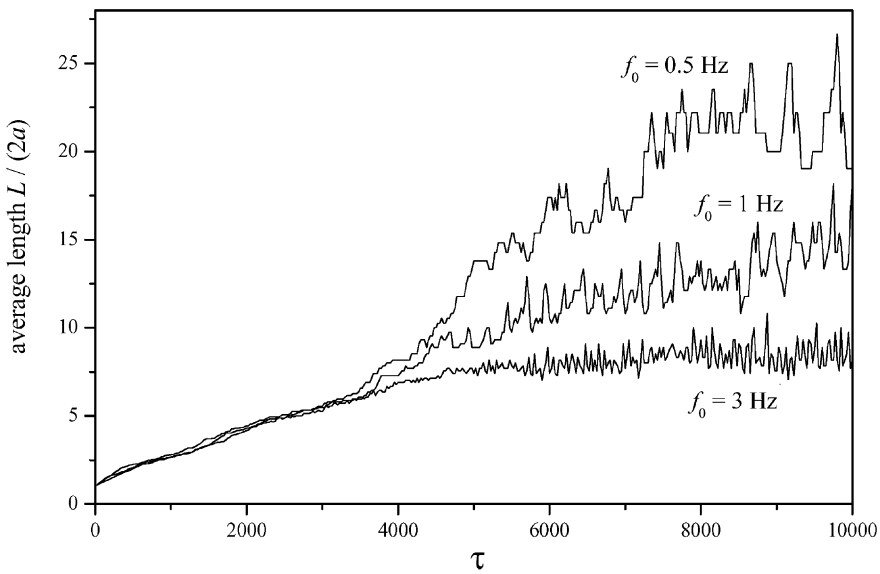

Fig. 9. Time evolution of the average length of the structures, L, at different rotating frequencies.

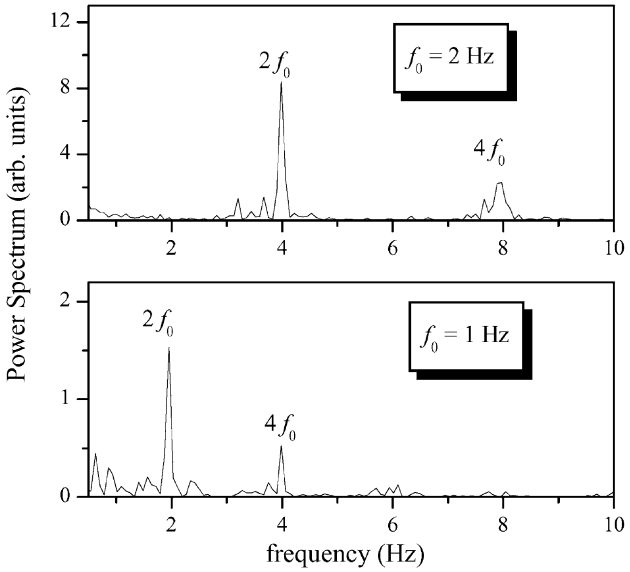

Fig. 10. Power spectrum of the average length of the structures, L, at different rotating frequencies. It is shown that the average length oscillates with a frequency two times the rotating field frequency ($2f_0$).

where L_0 is the steady state value, f_L the frequency of the modulated length, and ΔL the modulation amplitude. This frequency value, f_L, has been found to be related with the frequency of the rotating field, being two times the field frequency, $f_L = 2f_0$ (see Fig. 10). That means that on average, the chain-like structures break up (smallest size of L) and after a time they come together again (largest size of L) and this behavior is repeated two times every field cycle.

In Fig. 11, we show the steady state value of the average length, L_0, as a function of the rotating field

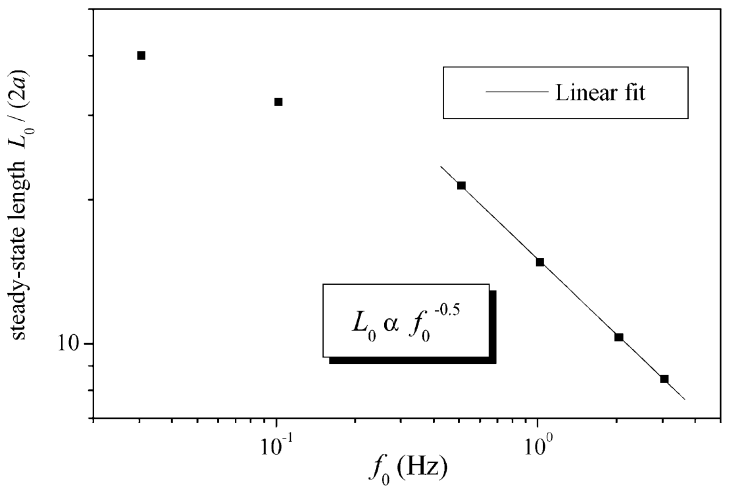

Fig. 11. Steady state length, L_0, vs. rotating field frequency.

frequency. At high frequencies this length L_0 follows a power law behavior with an exponent close to -0.5, in agreement with the experimental results. This is the same value found theoretically for steady simple shear and constant magnetic field when the shear rate is replaced with frequency [26]. In order to understand this exponent, we developed a simulation starting with a long individual chain, and calculated the maximum length for each rotational frequency that can follow the field without breaking up. We found that this length, that we called critical length L_c, follows a power law behavior with an exponent equal to -0.5, i.e. $L_c \propto f_0^{-0.5}$. This suggests that at high frequencies the steady state average length follows the same behavior than the critical length, it means that in this regime the size of the structures is governed by the hydrodynamic friction. As can be seen in Fig. 11, at small frequencies L_0 deviates from the above behavior. The change of the length with the frequency in this regime is relatively slow, in agreement with the experiments.

Acknowledgements

This research was partially supported by DGICYT (Grant no. PB96-0148). We gratefully acknowledge T. Madrid for developing software to improve images quality and to calculate Hough Transform. We also thank J. Anseth for helping with image analysis.

References

[1] G. Helgesen, P. Pieranski, A.T. Skjeltorp, Phys. Rev. Lett. 64 (1990) 1425.
[2] G. Helgesen, P. Pieranski, A.T. Skjeltorp, Phys. Rev. A 42 (1990) 7271.
[3] J.C. Bacri, A. Cebers, R. Perzynski, Phys. Rev. Lett. 72 (1994) 2705.
[4] O. Sandre, J. Browaeys, R. Perzynski, J.C. Bacri, V. Cabuil, R.E. Rosensweig, Phys. Rev. E 59 (1999) 1736.
[5] B.E. Kashevsky, A.L. Novokova, Magnetohydrodynamics 25 (1989) 304.
[6] S. Melle, G.G. Fuller, M.A. Rubio, Phys. Rev. E 61 (2000) 4111.
[7] K.B. Migler, R.B. Meyer, Phys. Rev. E 48 (1993) 1218.
[8] C. Zheng, R.B. Meyer, Phys. Rev. E 55 (1997) 2882.
[9] H.C. van de Hulst, Light Scattering by Small Particles, Dover, New York, 1981.
[10] M. Whittle, J. Non-Newtonian Fluid Mech. 37 (1990) 223.
[11] J.R. Melrose, D.M. Heyes, J. Chem. Phys. 98 (1993) 5873.
[12] M. Mohebi, N. Jamasbi, G.A. Flores, J. Liu, Int. J. Mod. Phys. B 13 (1999) 2060.
[13] J.E. Martin, R.A. Anderson, C.P. Tigges, J. Chem. Phys. 110 (1999) 4854.
[14] M. Mohebi, N. Jamasbi, J. Liu, Phys. Rev. E 54 (1996) 5407.
[15] J.E. Martin, R.A. Anderson, C.P. Tigges, J. Chem. Phys. 108 (1998) 3765, 7887.
[16] G. Bossis, J.F. Brady, J. Chem. Phys. 80 (1984) 5141.
[17] R.T. Bonnecaze, J.F. Brady, J. Chem. Phys. 96 (1992) 2183.
[18] Y. Baxter-Drayton, J.F. Brady, J. Rheol. 40 (1996) 1027.
[19] A. Satoh, R.W. Chantrell, G.N. Coverdale, S. Kamiyama, J. Colloid Interf. Sci. 203 (1998) 233.
[20] D.J. Klingenberg, F. van Swol, C.F. Zukovski, J. Chem. Phys. 91 (1989) 7888.
[21] J.F. Canny, IEEE Tans. Pattern Anal. Machine Intell. 8 (1986) 679.
[22] R.C. Gonzalez, R.E. Woods, Digital Image Processing, Addison-Wesley, Reading, MA, 1992 (Chapter 7).
[23] J.E. Martin, E. Venturini, J. Odinek, R.A. Anderson, Phys. Rev. E 61 (2000) 2818.
[24] J.E. Martin, Phys. Rev. E 63 (2000) 011406.
[25] R.G. Larson, The Structure and Rheology of Complex Fluids, Oxford University Press, New York, 1999.
[26] J.E. Martin, et al., J. Chem. Phys. 104 (1996) 4814.